Harris Cooper, William (Orcid ID: 0000-0002-9603-0014)
Miller Meghan, Samantha (Orcid ID: 0000-0001-5494-2296)
Supendi Pepen (Orcid ID: 0000-0002-9784-9865)
Widiyantoro Sri (Orcid ID: 0000-0002-8941-7173)

Subducted Lithospheric Boundary Tomographically Imaged beneath Arc-Continent Collision in Eastern Indonesia

Cooper W. Harris[1], Meghan S. Miller[2], Pepen Supendi[3], Sri Widiyantoro[4, 5]

[1] Department of Earth Science, University of Southern California, Los Angeles, CA, USA
[2] Research School of Earth Sciences, Australian National University, Canberra, ACT, Australia
[3] Agency for Meteorology, Climatology, and Geophysics (BMKG), Bandung, Indonesia
[4] Global Geophysics Research Group, Institut Teknologi Bandung, Bandung, Indonesia
[5] Faculty of Engineering, Maranatha Christian University Bandung, Bandung, Indonesia

Corresponding author: Cooper W. Harris (cwharris@usc.edu)

Key Points

- New dataset produces finite frequency P wave tomographic model with unparalleled resolution of young arc-continent collision in Indonesia.
- This model resolves a continuous slab that is deformed near the boundary between continental and oceanic crust but not torn.
- This implies deep continental subduction prior to slab tearing and the localization of deformation along compositional boundaries.

This article has been accepted for publication and undergone full peer review but has not been through the copyediting, typesetting, pagination and proofreading process which may lead to differences between this version and the Version of Record. Please cite this article as doi: 10.1029/2019JB018854

Abstract
We use travel-times from a temporary seismic deployment of 30 broadband seismometers and a national catalog of arrival times to construct a finite frequency teleseismic P-wave tomographic model of the upper mantle beneath eastern Indonesia, where subduction of the Indo-Australian plate beneath the Banda Arc transitions to arc-continent collision. The change in tectonics is due to a change from oceanic to continental lithosphere in the lower plate as inferred from geologic mapping and geophysical, geochemical, and geodetic measurements. At this inferred transition, we seismically image the subducted continent-ocean boundary at upper mantle depths that links volcanism on Flores to amagmatic orogenesis on Timor. Our tomographic images reveal a relatively high velocity feature within the upper mantle, which we interpret as the subducted Indo-Australian slab. The slab appears continuous yet deformed as a result of the change in buoyancy due to the composition of the incoming continental lithosphere. Accordingly, there is a difference in dip angle between the oceanic and continental sections of the slab albeit not a gap or discontinuity. We suggest the slab has deformed without tearing to accommodate structural and kinematic changes across the continent-ocean boundary as the two sections of the slab diverge. These results suggest that deformation in tectonic collisions can be localized along a continent-ocean boundary, even at depth. We propose that future slab tearing may develop where we observe slab deformation in our study region and that a similar process may take place in collisions generally.

1. Tectonic Setting

Eastern Indonesia marks the collision between the Australian continental margin and the Banda volcanic arc (e.g. Audley-Charles, 1968; Carter et al., 1976; Harris et al., 2009; Harris, 2011) (Figure 1). This collision is similar to ancient collisional events that are preserved in the geologic record as well as more advanced collisions unfolding in the Mediterranean and the Caribbean, for example (e.g. Govers and Wortel, 2005). The Banda Arc-Australia collision is remarkable, though, because of how immature it is which provides a glimpse into the evolution of syn-collisional mountain building and the end-stages of subduction (e.g. Karig et al., 1987; Keep and Haig, 2010; Tate et al., 2015; Saqab et al., 2017).

West of the islands of Flores and Sumba, the lower plate is composed of oceanic lithosphere, which subducts beneath the Sunda arc at a velocity ~70 mm/yr in a NNE direction (e.g. Tregoning et al., 1994; Nugroho et al., 2009) (Figure 2). To the east the composition of the lower plate changes to continental lithosphere, which collides with the Banda forearc and drives mountain building on the island of Timor (e.g. Audley-Charles, 1968, 2004; Bowin et al., 1980; Harris, 1991) (Figure 2). Timor itself is composed of Asian and Australian sedimentary sequences that have been sutured together and uplifted by the collision from submarine basins to elevations approaching 3 km in Timor-Leste (e.g. Audley-Charles, 1968; Harris et al., 2000; Tate et al., 2014).

Northward subduction along the Sunda has been ongoing for some ~45 Ma (e.g. Hall, 2002; Spakman and Hall, 2010). Sometime around 23 Ma Jurassic oceanic crust arrived at the Java trench, ultimately causing rapid slab rollback, trench retreat, oceanic spreading in the Banda Sea, and arc lengthening beginning ~16 Ma (Spakman and Hall, 2010; Hinschberger et al. 2001). Around 3-5 Ma, the Australian continental margin collided with the Banda arc near Timor (Bowin et al., 1980; Audley-Charles, 1986, 2004; Scotney et al., 2005; Harris, 2011). After the collision began, volcanism ceased on the islands of Wetar (3 Ma), Romang (1.7 Ma), Alor (1.3 Ma), and the Pantar Strait (<1 Ma) (e.g. Abbot and Chamalaun, 1981;

Honthaas et al., 1998; Elburg et al., 2004;) (Figure 2). Igneous samples from these islands have multiple isotopic ratios indicative of continental contamination, i.e. the presence of distinctly continentally derived material in island-arc magmas (e.g. Hilton and Craig, 1989; Hilton et al., 1992; Vroon et al., 1993; Hoogewerff et al., 1997; Honthaas et al., 1998) (Figure 1). The presence of continental isotopic signatures in the island volcanics is interpreted as the result of melting both upper and lower Australian continental crust beneath the arc, which, if this crust were emplaced by subduction, would require subduction to melting depths (Elburg et al. 2004, 2005; Honthaas et al., 1998). Similar analysis has documented continental contamination as far west as Flores (Elburg et al., 2005). The same isotopic ratios have been alternatively interpreted as stemming from local continental crust that has melted beneath volcanoes and not necessarily from continental lithosphere emplaced by continental subduction. Such an example includes the island of Ambon in the northern Banda Sea (Vroon et al., 2001). Other evidence for continental subduction includes the amount of shortening observed at the Timor Trough through seismic profiles and geologic mapping (Karig et al., 1987; Shulgin et al., 2009; Keep and Haig, 2010; Saqab et al, 2017). Balanced cross sections across East Timor (Timor-Leste) reveal >300 km of shortening between Timor and the incoming Australian plate and surmise that >200 km of Australian continental lithosphere has subducted (Tate et al., 2015). Finally, plate reconstruction modeling that synthesizes geophysical, geochemical, and geologic studies also suggests that 150-250 km of Australian continental material have subducted at the Timor-Tanimbar Trough (Hinschberger et al., 2005).

Certain plate reconstruction models indicate that, as recently as the Pliocene, subduction was active at the Timor Trough (e.g. Karig et al., 1987; Hinschberger et al., 2005). This is consistent with seismic reflection profiles suggesting that no subduction of the Australian continent has taken place at the now locked Timor Trough since ~0.5-1.0 Ma (Richardson and Blundell, 1996; Hughes et al., 1996). Other models, however, suggest there was never subduction at the Timor Trough, which was never a trench but rather an incipient foreland basin or foredeep (e.g. Hall, 2002, 2012; Audley-Charles, 2004; Keep and Haig, 2010; Spakman and Hall, 2010; Saqab et al., 2017). Indeed, certain plate reconstruction models indicate that, prior to the collision, subduction did occur at the paleo-plate boundary in this region, which was slightly north of the Timor Trough, but that this trench has since been overprinted and deformed and is now locked (Hall, 2012; Spakman and Hall, 2010). For the purposes of our deeper analysis, however, whether subduction of continental material occurred at the Timor Trough or a paleo-plate boundary is not particularly significant. The more relevant consideration is simply that continental material has subducted beneath the collision zone.

Recent convergence between Timor and Australia seems to be accounted for not by subduction, but by backarc thrusting and accretion (McCaffrey, 1996; Nugroho et al., 2009). This contrasts with the Sunda arc, where subduction of oceanic lithosphere continues at a rate of ~70 mm/year (Tregoning et al., 1994; Kreemer et al., 2000; Nugroho et al., 2009). These measurements agree with plate reconstruction and numerical modeling studies that predict the cessation of subduction in response to continental subduction at the Banda Arc specifically (Hinschberger et al., 2005; Royden and Husson, 2009). Thus, as shortening continues to uplift the sub-aerial forearc, subduction has arrested at the collisional front, whereas subduction continues further west, where no buoyant indenters resist sinking.

2. Data

Our dataset consists of ~20,000 arrival times of teleseismic P and PP waves recorded across Indonesia (Table 1). We manually picked P and PP arrival times from 207 events recorded across the YS network of 31 broadband stations (Miller et al., 2016) between 2014 and 2017 for a total of 9,838 travel time residuals (Figure 2). To this we added 10,117 automatically picked arrivals from 339 events recorded across 59 stations from the AU, IA, and II broadband seismic networks between 2010 and 2018 (Table 1, Figure 2). These data were provided by the Meteorological, Climatological, and Geophysical Agency (BMKG) headquartered in Jakarta, Indonesia. Automatic arrivals were picked using SeisComP3 software using a short-term-average/long-term-average (*sta*/*lta*) trigger on broadband data filtered between 0.7-2.0 Hz. We obtained travel-time residuals using predictions from the global one-dimensional velocity model *iasp91* (Kennett and Engdahl, 1991). To improve the quality of the manually picked residuals, we employed the cross-correlation optimization scheme of VanDecar and Crosson (1990) in four non-overlapping bandpasses (Table 1). Only measurements with cross-correlation coefficients ≥ 0.8 were used in the inversion. After pruning, all delays were demeaned per event.

Our input data is a vector of relative P-wave velocity perturbations. We solve for a tomographic model using inverse methods that relate seismic travel-times to three-dimensional lithospheric structure centered beneath the YS network (Miller et al., 2016) of seismometers (e.g. Aki et al., 1977; Nolet, 1987; Spakman, 1991). In addition to structure, seismic tomography is a suitable tool to constrain active mantle processes such as convection and lithospheric deformation (e.g. Wortel and Spakman, 2000; Schmandt and Humphreys, 2010a, 2010b).

3. Methods

Our data preparation produces a vector of travel-time residuals, **y**, which we use to solve a classical linear inverse problem:

$$y = Ax \tag{1}$$

where **A** is a matrix that maps between the elements of **y** and **x**, which contains coefficients of relative slowness (*i.e. velocity*$^{-1}$) perturbation for the set of basis functions that discretize the volume of Earth we wish to image (e.g. Spakman and Nolet, 1988; Trampert, 1998). **A** contains coefficients that describe the sensitivity of each measurement in our data vector **y** to each element of our model vector **x** (Table 2), accordingly, **A** reflects how thoroughly and how evenly our data sample the model space. The matrix **A** also contains coefficients to correct for the effects of errors in earthquake location and timing as well as the effects of shallow structure that our inversion cannot resolve (e.g. Aki 1977; Spakman et al., 1993). As we demeaned all residuals per event, the sum of all residuals is null and the final velocity model is one of relative perturbations (e.g. VanDecar and Crosson, 1990).

In a ray-theoretical approach, these sensitivity paths are one-dimensional. However, we employ a finite-frequency approach that utilizes three-dimensional sensitivity kernels (Dahlen et al., 2000). Finite-frequency tomography exploits the fact that seismic waves are sensitive to structure that is adjacent to the ray-theoretical travel-path. This sensitivity function is approximated as a 3D Fréchet differential kernel, which is roughly banana-shaped and describes the sampling relationship between a seismic wave and the voxels in a discretized mesh (Zhao et al., 2000). The width of each kernel is inversely related to the frequency band the kernel is calculated in (Hung et al., 2000), so different bandpasses are sensitive to different volumes of the mesh and contribute unique sampling information to the

inversion (e.g. Scire et al., 2016). Kernels for manually picked data were computed in four non-overlapping bandpasses. Kernels for the automatically picked data were computed in the same bandpass used by the automatic picking algorithm.

No inverse exists for **A** or $\mathbf{(A^TA)}$ and no unique solution exists to equation (1). This is due to sparsity of **A** and the fact that geophysical inversions are inherently underdetermined (e.g. Backus and Gilbert, 1967). This is also a natural consequence of using a truncated set of basis functions to infer a discretized model, **x**, that is actually continuous in the real Earth (Trampert, 1998). To help solve the multi-mapping (*i.e.* non-uniqness) that arises from our ill-posed problem, we use a Tikhonov regularization scheme to improve the conditioning of the problem by penalizing the L_2 norm (Euclidean length) of **x** during the inversion (e.g. Tikhonov, 1963; Phillips & Fehler, 1991; Trampert, 1998). We also penalize the length of the roughness (Laplacian) of **x**, which we compute over the model space as the difference between the perturbation value of a given block and the average of the adjacent voxels (e.g. Nolet, 1987; Schmandt and Humphreys, 2010b). We scale the length and roughness penalties by two damping constants, alpha and beta, respectively. This equates to solving equation (2).

$$argmin_x\{||Ax-b||^2+\alpha^2||x||^2+\beta^2||\nabla^2 x||^2\} \quad (2)$$

The regularization parameters (alpha, beta) and station/event correction terms (which are built into **A** and **x**) in equation (2) are used to steer the inversion towards a model vector that is as small and smooth as possible while still fitting the data to an acceptable level. We seek a model that minimizes the misfit between expected and measured travel times yet does so without being physically unreasonable, *i.e.* we wish to avoid a model that is too discontinuous or contains velocity perturbations that are too large. In subduction zones, much of the velocity perturbation field is related to the temperature of the cool, down-going slab. Thus, we would expect relatively smooth velocity anomalies because thermal anomalies, such as slabs, diffuse smoothly in the mantle (e.g. Minear & Toksöz, 1970; Mitronovas & Isacks, 1971; Kincaid & Sacks, 1997; van Keken et al., 2002). The regularization terms have an appreciable impact on the inversion process and represent non-linear tradeoffs in the final model. Thus, we iterated over a range of values for each parameter before choosing the combination that produced the model of choice (e.g. Kissling et al., 2001).

To actually solve equation (2) for a model vector we employ the LSQR algorithm, which is an iterative conjugate gradient procedure (Paige and Saunders, 1982). This procedure is analytically equivalent to other conjugate-gradient least-squares methods but is preferable given how ill-conditioned the system is (Paige and Saunders, 1982) and has been successfully applied to seismic tomography (e.g. Nolet, 1985).

4. Resolution

We conducted three main resolution tests to assess the resolving power and reliability of the model before interpreting specific features. First, we performed a standard "checkerboard" test to visualize the ability of the model to recover edges and amplitudes of a physically meaningless pattern (Figure 3). The procedure of this test begins with constructing a synthetic input model, $\mathbf{x_s}$, which is composed of blocks that are each 1° x 1° horizontally and 150 km thick and are uniformly ± 5% ∂Vp. The blocks alternate in polarity, evoking a 3D checkerboard. We then generate a vector of synthetic delay times, $\mathbf{\hat{y}_s}$, by multiplying the checkerboard model and the sampling matrix **A**. Next, we reinvert for the recovered synthetic model, $\mathbf{\hat{x}_s}$, using **A** and the same damping parameters from the real inversion. Finally, we compare $\mathbf{x_s}$ and $\mathbf{\hat{x}_s}$. Qualitatively good visual agreement between the input and recovered

synthetic models suggests spatial resolution on the order of, and coarser than, the input blocks. After performing this checkerboard test, we believe that the sub-region of the model comprising Flores, the Savu Sea, and Timor has sufficient resolution to interpret lithospheric-scale structure between 100-400 km depth.

Second, we recovered several synthetic input models that were designed to represent features of potential interest, such as a slab dipping at ~60 degrees into the mantle , a slab with a change in dip on either side of the continental-ocean boundary above 300 km depth, and a continuous dipping slab with a change in morphology at the continent-ocean boundary (Figure 4), and a slab that is divided by a 50 km vertical tear that extends to the surface. This procedure is similar to that of a checkerboard test in that we use a synthetic model vector to generate a synthetic delay vector, invert for a recovered synthetic model, and compare it to the input.

We believe these tests illustrate several key points: 1) Our model is capable of recovering a continuous or discontinuous slab spanning the Sunda-Banda transition and collision zone; 2) Our model is capable of recovering a continuous slab with a change in dip at the ocean-continent boundary at depth; 3) Perhaps most importantly, our model is capable of recovering a narrow slab gap that is only 2 voxels (~ 50 km) wide that extends from the surface to 200 km depth at the ocean-continent boundary near central Flores. The vertical slices taken at the hypothetical slab gap illustrate the significantly different models that would arise from a gap or not in a high-velocity slab. In short, if there were a slab gap or tear at the subduction-collision boundary, we are confident it would appear in the model.

Third, we visualize voxel sampling of our model as ray-theoretical hit-count. We note that the areas of the model we wish to interpret are well-sampled by rays and thus are also sampled by 3D kernels (Figure 5). We note, too, that there is a lack of resolution and sampling in various areas, the Banda Sea, northwest of Wetar and Timor, in particular. This is directly related to the lack of instruments beyond the major islands (Figures 1 and 2). Therefore, we do not interpret the model in these areas. However, due to the priority of well-sampled voxels in the inversion, unsampled regions of the mesh do not contain as much high-amplitude structure in the model as well-sampled areas. The most densely sampled voxels at 200 km depth underlie the Savu Sea, northern Timor, Flores, Alor, and Wetar; these areas correspond to the approximate location of the slab, as inferred from seismicity (e.g. Das, 2004). Thus, we believe the model is well suited to investigate the structure of the slab at upper mantle depths.

5. Results

At 100 km depth, we image a high velocity feature that extends from Bali to Romang (Figure 6). West of ~121º E this feature is oriented roughly E-W and extends from Bali to central Flores, underling the active arc. Further east, however, the feature strikes ESE-WNW and extends from the central Savu Sea to the island of Romang, underling the extinct volcanic arc and Timor. These two sections appear to have different dips, which is steeper in the east, and are connected at a step, or bend, beneath the Savu Sea ~122º E. The distance from the convergent plate boundary to the fast material is ~2x larger in the west, in agreement with that region having a lower dip. The connection point between the sections is approximately north of where the strike of the plate boundary bends toward the north. We note that the overall fast anomaly is coherent along strike, showing no signs of a gap or discontinuity. The anomaly does not extend east of Romang in our model and appears somewhat discontinuous west of Sumba. We attribute this mostly to a lack of sampling in this area at shallow depths (Figure 6).

At 200 km depth, the aforementioned two sections are still visually offset and still connected, forming a continuous, kinked feature (Figure 6). The boundary between them is ~122º E and, at this depth, directly underlies the isotopic continental contamination front in the active arc (Figure 1) (e.g. Hilton et al., 1992; Elburg et al., 2004; Fichtner et al., 2010). At this depth, the western section is comparably further north, which is consistent with a shallower dip angle. At 200 km, the fast material extends further east, into the Banda Sea, and is more continuous west of Sumba. The greater extent and continuity of the anomaly are consistent with increased lateral sampling with depth due to the curving ray paths and sensitivity kernels.

At 300 km depth, the eastern and western sections of the high velocity anomalies are no longer clearly distinguishable from one another and appear to merge into an anomaly with a consistent dip (Figure 6). There is a slight change in morphology ~121.5º E, though this does not correspond to a clear offset as seen in the shallower slices. At this depth, the anomaly underlies both active and inactive sections of the arc and extends even further east into the Banda Sea. The dip of the anomaly is less steep compared to shallower depths and the anomaly is more extensive in the north-south direction. The feature at this depth extends from beneath Bali to the Banda Sea.

Figure 7 presents longitudinal cross-sections taken east of, at, and west of the change in dip described in the depth-slices. In these panels, we observe the same northward dipping high velocity anomaly described above (Figure 6). In all three cross-sections, the fast material extends from the top to the bottom of the model although there is a weaker fast signal in the most eastern slice. We note that the dipping feature generally coincides with regional Wadati-Benioff zone seismicity ($m_w \geq 4.5$, 1990-2019) which is plotted within ± 1º longitude from each cross-section (Figure 7) (https://earthquake.usgs.gov/earthquakes/search/). Longitudinal cross-sections of the model taken at 122ºE and 124ºE reveal a high velocity material with a relatively constant dip. These slices correspond to the collision zone. Further west, at 119ºE, where oceanic subduction is active, the fast anomaly has a shallower dip angle above ~ 200 km and a nearly vertical dip angle below ~ 200 km. This contrasts with the steep, uniform dip further east.

Finally, we acknowledge significant areas of slow velocities in our model. The apparent slow regions are generally in relatively well-resolved regions of our mesh and are generally on either side of fast velocity features we previously described. We do not dismiss the slow regions as being solely artifacts, though we do believe that, at upper mantle depths, the primary velocity anomalies in this region are due to high velocity downwellings corresponding to cold, subducted lithosphere. This is consistent with subduction zones globally (e.g. Kárason and van der Hilst, 2000).

6. Interpretations and Discussion

We relate the dipping, fast anomaly to the subducting Indo-Australian slab. This slab subducts beneath the Sunda and Banda arcs and contains both oceanic and continental lithosphere, which we will refer to as comprising the western and eastern sections of the overall slab, respectively. We infer that the change in slab morphology near central Flores is deep structural evidence of the ocean-continent boundary in the lower plate.

Previous tomographic models have helped constrain the upper mantle structure of the broader Indonesian region. The global models of Widiyantoro and van der Hilst (1996, 1997),

Bijwaard et al., (1998), and Amaru (2007) reveal a curvilinear Indo-Australian slab that penetrates deep into the mantle and in some regions into the lower mantle. These models address the greater Indonesian region and do not specifically focus on the ocean-continent boundary in the slab at depth. Also, because they are global inversions, they have coarser resolution (>1-2 degrees) than our model (~50 km) specifically in the Savu Sea area. Accordingly, these models do not exhibit a visible change in slab morphology across the subduction-collision transition. However, the general location and orientation of the slab in this study is consistent with the global models.

The regional model of Widiyantoro et al. (2011) uses a similar methodology and mesh to the current study and shares many common features with our model. Both reveal an arcuate slab that changes morphology with depth. In both models, at depths shallower than ~200 km, the slab extends relatively far north to the east of central Flores. This contrasts with Timor, where the collision is more advanced, but the slab does not extend as far north at this depth. This offset is not as prominent in either model below 250 km, at which point the northern extent of the slab is relatively smooth across the boundary of collisional onset. These similarities aside, the current study has higher resolution. For comparison, the model of Widiyantoro et al. (2011) has its best resolution at ~200 km depth, where it is capable of resolving input anomalies on the order of 2º x 2º in latitude and longitude. This is twice as coarse as our resolving power at the same depth (Figure 3). The current inversion has higher resolution (~50 km horizontally) despite having only < 20,000 arrival times as input data, which is much smaller than the data vector of Widiyantoro et al (2011), which uses > 950,000 travel times. This is due to the data from the YS seismic network, which is unique to this work, and samples regions of the mesh that would otherwise have no constraints due to a lack of instrumentation.

The regional P and S wave tomographic models of Zenonos et al. (2019) span the larger Indonesian region and make use of seismic stations across southeast Asia and Australia, though do not include the YS network. The models were constructed using global seismic catalogs, the “fast marching” eikonal tomographic method (e.g. Sethian and Popovici, 1999), andElburg et al., 2004Elburg et al., 2004 an unsupervised machine learning algorithm that clusters, prunes, and de-noises the travel-time dataset (Zenonos et al., 2019). The resulting models have horizontal resolution on the order of 130 km for the P wave models and 220 km for the S wave model, which is comparable to but still coarser than our resolution (Figure 3). Zenonos et al. (2019) do not image any gaps or tears beneath central Flores, where the slab is laterally continuous across the boundary of collisional onset at depths ≥ 300 km in their P and S models. They do, however, image a minor hole ~400 km depth beneath western Sumba and a vertically larger hole further west, beyond the edge of our model space. Our model, however, is continuous beneath Sumba (Figure 7*a*). We believe this disagreement is due to higher resolution in the present study, which, in turn, is due to higher instrumentation in the Sumba and west Flores region. Zenonos et al. (2019) relate the hole near Sumba to a discontinuity beneath east Java, which is potentially due to the subduction of a buoyant plateau that resulted in local slab detachment (Hall and Spakman, 2015). We suggest that the tear proposed by Hall and Spakman (2015) is too far west (~1000 km) to explain the discontinuities observed by Zenonos et al. (2019) and note that the global tomographic model of Amaru (2007), which was used by Hall and Spakman (2015), does not image robust lateral discontinuities near Sumba or Flores.

The regional tomographic model of Fichtner et al. (2010), which uses a full waveform inversion to invert for relative S wave velocity perturbations in the upper mantle, also images

a change in velocity that is interpreted as a change in lithospheric composition near central Flores. This study presents an excellent complement to the aforementioned work because our best resolution is between 100-300 km and we constrain P wave velocity perturbations, which are related to S-wave velocity perturbations through the bulk modulus, which both velocity equations contain. The full waveform model suggests that continental lithosphere has subducted beneath Timor and underlies much of the uplifted forearc as well as the active arc, where continental contamination has been observed geochemically (Hilton et al., 1992; Elburg et al., 2004, 2005). The western edge of the subducted continental lithosphere is found near central Flores, precisely where we observe a change in slab morphology (Shulgin et al., 2009; Fichtner et al., 2010). This agreement with the full waveform model further supports our interpretation of the offset in the western and eastern slabs occurring at the ocean-continent boundary.

We believe that the reason we see a change in slab morphology at this boundary is related to the compositional and kinematic differences of the down-going material. The Australian continental lithosphere is older, colder, and seismically faster than the Indian ocean subducting beneath the Sunda Arc and is on the order of 200 km thick (Fichtner et al., 2010; Goes et al., 2005). Subduction continues at a rate of ~ 70 mm/yr west of Sumba, but has ceased along the collisional front itself, as confirmed by GPS data and geologic observations of tectonic accretion (Tregoning et al., 1994; McCaffrey, 1996; Kreemer et al., 2000, Nugroho et al., 2009). Furthermore, a comprehensive analysis of plate motion reference frames reveals that the Sunda-Java trench is migrating northward and undergoing trench-advance, and that the velocity of trench advance tapers towards the collision zone, where the convergent plate boundary is stationary (Heuret and Lallemand, 2005; Becker et al., 2015). The buoyancy of the continental slab is driving the collision at the surface and we believe this deformation is integrated down to depths exceeding 200 km.

6.1 Steep Continental Slab

Above 200 km, the western slab has a shallower dip compared to beneath the collision, where dip is nearly vertical, suggesting a steeply dipping continental slab (Figure 7). This observation is consistent with earthquake catalogs that reveal a steeper slab near the collision zone, especially at shallower depths (Schöffel and Das, 1999; Das, 2004). In fact, a steeper continental slab could be explained by the semi-analytical model of Royden and Husson (2009), who studied the Banda-Australian collision in particular. Their model simulated the effects of continental subduction and found that, after subduction stopped, slab dip increased as the slab "folded", rotating about a hinge which is, at first, near the convergent plate boundary itself (Royden and Husson, 2009). Steep subduction has also been evoked in the western Himalaya, where thick, low density Indian continental lithosphere was bent into a tight radius of curvature as it resisted subduction prior to slab breakoff (Leech et al., 2005).

We suggest a steeper dip is reasonable for the subducted Australian continent as it is still attached to the oceanic lithosphere that preceded it in subduction. Deeper tomographic models, such as the P wave model presented by Widiyantoro and van der Hilst (1997) and Amaru (2007), image a continuous Indo-Australian slab down to depths exceeding the mantle transition zone (>660 km). Thus, there is a considerable amount of negative pull on the positively buoyant continent and the slab has not ruptured or undergone break-off in such a way that would vertically separate the continental and oceanic components. Subduction has ceased, but we believe the continental slab is tilting under the pull of the previously subducted ocean and that slab dip is increasing accordingly.

6.2 Slab Deformation

Overall, the arrival of the Australian continent at the convergent plate boundary has produced a gradient in subduction rate and slab dip across the Sunda-Banda subduction-collisional front. Gradients in subduction rate and slab dip are thought to drive deformation in subduction zones that eventually results in slab segmentation tearing (e.g. Doglioni et al., 1994; Rosenbaum et al., 2008; Govers and Wortel, 2005).

Tomographic imaging has been used to identify such tearing: In the Alboran Sea, a tear has propagated along northern Africa as the retreating Betic-Alboran slab detaches from the African continental margin, similar to the South American-Caribbean plate margin (Spakman and Wortel, 2004; Miller et al., 2009; Levander et al., 2014). Progressive collision between the Bahamas Plateau and the now volcanically extinct Greater Antilles arc has resulted in the cessation of subduction, the creation and divergence of microplates, differential rollback, and slab segmentation tearing (Meighan et al., 2013; Harris et al., 2018). Beneath Italy, the Tyrrhenian slab has undergone various episodes of lithospheric tearing as a consequence of multiple collisions between the arc and buoyant indenters (Rosenbaum et al., 2008). In the Mariana Arc region, the buoyant Caroline Island Ridge has collided with the trench and driven tearing by resisting subduction and increasing arc curvature (Miller et al., 2006). Thus, the collision in Banda may be driving tearing as a consequence of changing the kinematics (rate and dip) of subduction.

A critical element common to the tomographic models discussed above is that they all feature visible, lithospheric-scale slab gaps (or windows) in high-velocity structure that coincides with the inferred tearing and the tectonic/kinematic boundaries of interest. Conversely, our model does not resolve any along-strike gaps in the subducted lithosphere near the change from subduction to collision, nor along the ocean-continent boundary in the slab. As illustrated by the synthetic recovery test of a narrowly torn slab, we are confident that our model would contain a visibly distinguishable tear if it existed. Rather, the slab appears laterally continuous near central Flores, where our resolution is highest. In fact, no previous tomographic model of the upper mantle in this region has imaged a gap or inferred a tear near central Flores (Widiyantoro and van der Hilst, 1996, 1997; Bijwaard et al., 1998; Amaru, 2007; Widiyantoro et al., 2011; Zenonos et al., 2019).

Instead of tearing, we suggest that the stresses resulting from the different kinematics of the two slab sections are deforming the slab where the two sections meet. This would produce a thinned boundary that bridges the oceanic and continental regions, which have different dips and different subduction velocities. Thus, the overall deformation would include horizontal and vertical components in order to accommodate down-dip and along-strike divergence without a tear (Figure 8).

Slab deformation, which has been observed in arcuate subduction zones globally as a mechanism to accommodate increased arc curvature and arc length, has been identified as a predecessor to slab-tearing, but does not constitute a tear *per se* (e.g. Doglioni, 1991, Wortel and Spakman, 2000). The aforementioned examples of tearing in the Tyrrhenian-Apennines (Doglioni, 1991) and the Alboran (Faccenna et al., 2004) slabs are believed to have developed after slab stretching thinned the subducted lithosphere first. Elsewhere, tomographic imaging of the Juan de Fuca and Explorer slabs in the American Pacific northwest has led to the interpretation of slab stretching at depth as a response to plate reconfiguration at shallower levels (Audet et al., 2008). Stretching has been evoked at the

southern edge of the Juan de Fuca plate, as well, as a means to fill the gap left by the northward migration of the Mendocino triple junction (ten Brink et al., 1999).

Numerical modeling supports the ability of slabs in the upper mantle (above the mantle transition zone) to deform and accommodate extension without tearing (e.g. Hale et al., 2010; van Hunen and Allen, 2011). Subduction itself inherently requires deformation, such as bending, when a slab enters a trench and descends into the mantle (Ribe, 2001). Furthermore, the process of bending a viscous sheet is naturally accompanied by some level of stretching (Ribe, 2001). Variations in the forces that resist the viscous deformation of slabs are related to the speed and dip of subduction, as well as the tendency of slabs to stretch or bend (Houseman and Grubbins, 1997; Becker et al., 1999). While all slabs stretch to some extent, weaker, less viscous slabs are more prone to stretching than thicker, more viscous slabs (Capitanio et al., 2007). Thus, as the ocean-continent boundary undergoes non-tearing deformation, this deformation may unfold differently in the two regions of the slab due to different ages, thicknesses, and viscosities.

In eastern Indonesia specifically, slab stretching has already been observed, albeit further east. Since ~16 Ma, the arrival of Jurassic oceanic crust at the Sunda-Java trench has caused rapid slab rollback in the Banda Sea, resulting in the near 180º of curvature the modern Banda Arc (e.g. Hall, 2001; Spakman and Hall, 2010; Hall, 2012). As the slab rolled back, extension in the overriding plate drove seafloor spreading in the south Banda basin (e.g. Honthaas et al., 1999; Charlton, 2000; Harris et al., 2006). The lower plate experienced extension and thinning as well as the slab stretching at depth to eventually achieve a spoon-shape as the arc lengthened and became more highly curved (Spakman and Hall, 2010).

Overall, our tomographic model does not image a tear. Given modeling results and studies of other subduction zones, we advocate deformation without tearing. We suggest that, while the Indo-Australian slab has not yet torn at the subducted ocean-continent boundary at depth, a tear may develop in the future. We suggest the extent of deformation that would precede such a tear but we do note the 3D numerical modeling work of Menant et al. (2016), which invokes slab stretching as a precursor to tearing of a subducted continental material in order to explain trench migration and magma genesis in the eastern Mediterranean. Furthermore, we believe that the oceanic and continental sections of the slab are undergoing different amounts of bending and stretching due to their material properties and that the oceanic side of the boundary may be stretching more/more quickly.

6.3 Slab Breakoff

Controversy exists surrounding the presence of a horizontal slab breakoff tear near Timor. Elburg et al. (2004) found isotopic signatures of Australian lower crust in igneous rocks near the collision zone and suggested horizontal slab breakoff below magmagenic depths (100-150 km) to explain the heat influx required to melt the lower crust. Sandiford (2008) and Ely and Sandiford (2010) used earthquake data to infer a slab detachment along a horizontal tear ≤100 km beneath western Timor ~124ºE. Reasoning for such a tear includes alternating regions of down-dip tension and compression in the slab from intermediate depth seismicity (Ely and Sandiford, 2010). Indeed, such a detachment would explain intermediate seismic quiescence near eastern Timor (Das, 2004) as well as variations in seismic moment release across the collision zone (Sandiford, 2008). However, our model does not resolve any horizontal gaps in high velocity material that are consistent with break-off or slab detachment. Cross-section *C* from Figure 7 corresponds to the location of the proposed tear in Ely and Sandiford (2008), yet we see no evidence of vertical gaps between 50-100 km. Thus, we do not support the

existence of slab detachment beneath Timor. However, Ely and Sandiford (2008) do identify a change in in-slab stresses as well as a region of tensile slab-thinning that overlaps nicely with the deformation in our tomographic model and is consistent with non-tearing deformation. For slab-breakoff to explain seismic quiescence, the slab would have to sink beyond seismogenic depths. Given the young age of the collision we find that this is not a suitable explanation for the region at hand. We propose that the anomalous seismicity stems from internal slab deformation and that the low rate of intermediate earthquakes is due to the cessation of subduction where the collision is most advanced.

7. Conclusions

The collision between the Banda Arc and the Australian continental margin is remarkable because of the active deep continental subduction and along-strike gradient from subduction to collision. We tomographically image a continuous subducting slab across the boundary between oceanic and continental lithosphere in the lower plate at upper mantle depths. We accomplish this using an array of permanent seismometers in Indonesia, which is augmented by a targeted, temporary deployment of 30 broadband stations across the collision zone. Our model offers unprecedented resolution across the ocean-continent transition in the lower plate because it is the first such model to include data recorded on the YS broadband seismic network.

We image a continuous, subducted slab that includes both oceanic and continental lithosphere. These two sections are visually distinguishable above ~250 km and are joined at a kink that overlaps the ocean-continent boundary in the lower plate. A change in slab morphology is collocated with a kinematic transition from subduction and trench-advance in the west to collision and a stationary convergent plate boundary in the east. We relate this to the change in dip between different regions of the overall slab as the continental section is steeper than the oceanic. We suggest the slab is deforming, but not tearing, near the lithospheric boundary and that oceanic lithosphere is primarily accommodating the relevant extension.

The spatial overlap between the slab deformation and the compositional boundary in the subducting Australian lithosphere is indicative of the correlation between physical heterogeneities and slab-deformation in subduction zones generally. Indeed, slab deformation in the Banda Arc-Australia collision is localized along the division between regions of different buoyancy and viscosity. While tearing has not yet begun, segmentation style tearing may very well succeed the observed deformation. This supports the notion that the location and configuration of future slab tearing can be predicted with knowledge of compositional partitions in subducting lithosphere. Additionally, we see no tomographic evidence for slab detachment beneath Timor and challenge the theory that breakoff has occurred.

Finally, this paper illustrates the efficacy of using targeted temporary seismic deployments to augment imaging resolution in body-wave tomographic models of curvilinear features, such as island arcs. Our model uses fewer data points than a recent study using a similar technique, but we achieve higher resolution due to new island stations overlying previously unsampled volumes of the model space.

8. Acknowledgements

We would like to thank the *Badan Meteorologi, Klimatologi, dan Geofisika* (BMKG) for access to Indonesian earthquake catalogs. We also thank the *Instituto do Petróleo e Geologia* (IPG) of Timor-Leste, without their fieldwork support this work would not have been

possible. Specifically we would like to thank the field team, including Nova Roosmawati, Leland O'Driscoll, Eugénio Soares, Luís Teófilo da Costa, and Robert Porritt. This work was funded by NSF grant EAR-1250214 as well as DIKTI grant 127/SP2H/PTNBH/DRPM/2018. All data used to create the velocity model in this publication are freely available for download on Dryad (doi:10.5061/dryad.w3r2280mv).

References

Abbot, M. J., & Chamalaun, F. H., 2nd. (1981). Geochronology of some Banda Arc volcanics. *The Geology and Tectonics of Eastern Indonesia*, 253–268.

Aki, K., Christoffersson, A., & Husebye, E. S. (1977). Determination of the three-dimensional seismic structure of the lithosphere. *Journal of Geophysical Research*, *82*(2), 277–296. https://doi.org/10.1029/JB082i002p00277

Amaru, M. L. (2007). *Global travel time tomography with 3-D reference models* (PhD Thesis). Utrecht University.

Audet, P., Bostock, M. G., Mercier, J.-P., & Cassidy, J. F. (2008). Morphology of the Explorer–Juan de Fuca slab edge in northern Cascadia: Imaging plate capture at a ridge-trench-transform triple junction. *Geology*, *36*(11), 895–898. https://doi.org/10.1130/G25356A.1

Audley-Charles, M. G. (1986). Rates of Neogene and Quaternary tectonic movements in the Southern Banda Arc based on micropalaeontology. *Journal of the Geological Society*, *143*(1), 161–175.

Audley-Charles, M. G. (2004). Ocean trench blocked and obliterated by Banda forearc collision with Australian proximal continental slope. *Tectonophysics*, *389*(1–2), 65–79.

Audley-Charles, Michael Geoffrey. (1968). The geology of Portuguese Timor: Geol. *Soc. London Mem*, *4*, 74.

Backus, G. E., & Gilbert, J. F. (1967). Numerical applications of a formalism for geophysical inverse problems. *Geophysical Journal International*, *13*(1–3), 247–276.

Becker, T. W., Schaeffer, A. J., Lebedev, S., & Conrad, C. P. (2015). Toward a generalized plate motion reference frame. *Geophysical Research Letters*, *42*(9), 3188–3196.

Becker, Thorsten W., Faccenna, C., O'Connell, R. J., & Giardini, D. (1999). The development of slabs in the upper mantle: Insights from numerical and laboratory experiments. *Journal of Geophysical Research: Solid Earth*, *104*(B7), 15207–15226.

Bijwaard, H., Spakman, W., & Engdahl, E. R. (1998b). Closing the gap between regional and global travel time tomography. *Journal of Geophysical Research: Solid Earth*, *103*(B12), 30055–30078. https://doi.org/10.1029/98JB02467

Bird, P. (2003). An updated digital model of plate boundaries. Geochemistry, Geophysics, Geosystems, 4(3), 1027. https://doi.org/10.1029/ 2001GC000252

Bowin, C., Purdy, G. M., Johnston, C., Shor, G., Lawver (5), L., Hartono (6), H. M. S., & Jezek (7), P. (1980). Arc-Continent Collision in Banda Sea Region. *AAPG Bulletin*, *64*(6), 868–915.

Capitanio, F. A., Morra, G., & Goes, S. (2007). Dynamic models of downgoing plate-buoyancy driven subduction: Subduction motions and energy dissipation. *Earth and Planetary Science Letters*, *262*(1–2), 284–297.

Carter, D. J., Audley-Charles, M. G., & Barber, A. J. (1976). Stratigraphical analysis of island arc—continental margin collision in eastern Indonesia. *Journal of the Geological Society*, *132*(2), 179–198.

Charlton, T. R. (2000). Tertiary evolution of the Eastern Indonesia Collision Complex. *Journal of Asian Earth Sciences*, *18*(5), 603–631. https://doi.org/10.1016/S1367-9120(99)00049-8

Dahlen, F. A., Hung, S.-H., & Nolet, G. (2000). Fréchet kernels for finite-frequency traveltimes—I. Theory. *Geophysical Journal International*, *141*(1), 157–174. https://doi.org/10.1046/j.1365-246X.2000.00070.x

Das, S. (2004). Seismicity gaps and the shape of the seismic zone in the Banda Sea region from relocated hypocenters. *Journal of Geophysical Research: Solid Earth*, *109*(B12), B12303. https://doi.org/10.1029/2004JB003192

Doglioni, C. (1991). A proposal for the kinematic modelling of W-dipping subductions-possible applications to the Tyrrhenian-Apennines system. *Terra Nova*, *3*(4), 423–434.

Doglioni, Carlo, Mongelli, F., & Pieri, P. (1994). The Puglia uplift (SE Italy): an anomaly in the foreland of the Apenninic subduction due to buckling of a thick continental lithosphere. *Tectonics*, *13*(5), 1309–1321.

Elburg, M. A., Van Bergen, M. J., & Foden, J. D. (2004). Subducted upper and lower continental crust contributes to magmatism in the collision sector of the Sunda-Banda arc, Indonesia. *Geology*, *32*(1), 41–44.

Elburg, M. A., Foden, J. D., Van Bergen, M. J., & Zulkarnain, I. (2005). Australia and Indonesia in collision: geochemical sources of magmatism. *Journal of Volcanology and Geothermal Research*, *140*(1–3), 25–47.

Ely, K. S., & Sandiford, M. (2010). Seismic response to slab rupture and variation in lithospheric structure beneath the Savu Sea, Indonesia. *Tectonophysics*, *483*(1–2), 112–124. https://doi.org/10.1016/j.tecto.2009.08.027

Faccenna, C., Piromallo, C., Crespo-Blanc, A., Jolivet, L., & Rossetti, F. (2004). Lateral slab deformation and the origin of the western Mediterranean arcs. *Tectonics*, *23*(1), TC1012. https://doi.org/10.1029/2002TC001488

Fichtner, A., De Wit, M., & van Bergen, M. (2010). Subduction of continental lithosphere in the Banda Sea region: Combining evidence from full waveform tomography and isotope ratios. *Earth and Planetary Science Letters*, *297*, 405–412. https://doi.org/10.1016/j.epsl.2010.06.042

Gasparon, M., Hilton D. R., Varne, R. (1994). Crustal contaminatino processes traced by helium isotopes: Examples from the Sunda arc, Indonesia. *Earth and Planetary Science Letters*, *126*(15–22).

Goes, S., Simons, F. J., & Yoshizawa, K. (2005). Seismic constraints on temperature of the Australian uppermost mantle. *Earth and Planetary Science Letters*, *236*(1–2), 227–237.

Govers, R., & Wortel, M. J. R. (2005). Lithosphere tearing at STEP faults: response to edges of subduction zones. *Earth and Planetary Science Letters*, *236*(1), 505–523. https://doi.org/10.1016/j.epsl.2005.03.022

Hale, A. J., Gottschaldt, K.-D., Rosenbaum, G., Bourgouin, L., Bauchy, M., & Mühlhaus, H. (2010). Dynamics of slab tear faults: Insights from numerical modelling. *Tectonophysics*, *483*(1–2), 58–70.

Hall, R. (2001). Extension during late Neogene collision in east Indonesia and New Guinea. *Journal of the Virtual Explorer*, *4*, 1–14.

Hall, R. (2002). Cenozoic geological and plate tectonic evolution of SE Asia and the SW Pacific: computer-based reconstructions, model and animations. *Journal of Asian Earth Sciences*, *20*(4), 353–431. https://doi.org/10.1016/S1367-9120(01)00069-4

Hall, R. (2012). Late Jurassic–Cenozoic reconstructions of the Indonesian region and the Indian Ocean. *Tectonophysics*, *570-571*, 1-41.

Hall, R., & Spakman, W. (2015). Mantle structure and tectonic history of SE Asia. *Tectonophysics*, *658*, 14–45.

Harris, C. W., Miller, M. S., & Porritt, R. W. (2018). Tomographic Imaging of Slab Segmentation and Deformation in the Greater Antilles. *Geochemistry, Geophysics, Geosystems*, *19*(8), 2292–2307.

Harris, R. (2011). The Nature of the Banda Arc–Continent Collision in the Timor Region. In *Arc-Continent Collision* (pp. 163–211). Springer, Berlin, Heidelberg. https://doi.org/10.1007/978-3-540-88558-0_7

Harris, R. A. (1991). Temporal distribution of strain in the active Banda orogen: a reconciliation of rival hypotheses. *Journal of Southeast Asian Earth Sciences*, *6*(3–4), 373–386. https://doi.org/10.1016/0743-9547(91)90082-9

Harris, Ron. (2006). Rise and fall of the Eastern Great Indonesian arc recorded by the assembly, dispersion and accretion of the Banda Terrane, Timor. *Gondwana Research*, *10*(3), 207–231. https://doi.org/10.1016/j.gr.2006.05.010

Harris, R., Kaiser, J., Hurford, A., & Carter, A. (2000). Thermal history of Australian passive margin cover sequences accreted to Timor during Late Neogene arc–continent collision, Indonesia. *Journal of Asian Earth Sciences*, *18*(1), 47–69.

Harris, Ron, Vorkink, M. W., Prasetyadi, C., Zobell, E., Roosmawati, N., & Apthorpe, M. (2009). Transition from subduction to arc-continent collision: Geologic and neotectonic evolution of Savu Island, IndonesiaTransition from subduction to arc-continent collision. *Geosphere*, *5*(3), 152–171. https://doi.org/10.1130/GES00209.1

Heuret, A., and S. Lallemand (2005), Slab dynamics and back-arc deformation, *Physics of the Earth and Planetary Interiors*, 149, 31–51. https://doi.org/10.1016/j.pepi.2004.08.022

Hilton, D. R., & Craig, H. (1989). A helium isotope transect along the Indonesian archipelago. *Nature*, *342*(6252), 906–908. https://doi.org/10.1038/342906a0

Hilton, D. R., Hoogewerff, J. A., Van Bergen, M. J., & Hammerschmidt, K. (1992). Mapping magma sources in the east Sunda-Banda arcs, Indonesia: constraints from helium isotopes. *Geochimica et Cosmochimica Acta*, *56*(2), 851–859.

Hinschberger, F., Malod, J.-A., Réhault, J.-P., Villeneuve, M., Royer, J.-Y., & Burhanuddin, S. (2005). Late Cenozoic geodynamic evolution of eastern Indonesia. *Tectonophysics*, *404*(1–2), 91–118.

Hinschberger, F., Malod, J.A., Dyment, J., Honthaas, C., Rehault, J.P. & Burhanuddin, S. 2001. Magnetic lineations constraints for the back-arc opening of the Late Neogene South Banda Basin (eastern Indonesia). Tectonophysics, 333 (1-2), 47-59.

Honthaas, C., Réhault, J.-P., Maury, R. C., Bellon, H., Hémond, C., Malod, J.-A., Cornée, J.-J., Villeneuve, M., Cotten, J., Burhanuddin, S., Guillou, H. & Arnaud, N. (1998). A Neogene back-arc origin for the Banda Sea basins: geochemical and geochronological

constraints from the Banda ridges (East Indonesia), *Tectonophys.* 298, 297-317. https://doi.org/10.1016/S0040-1951(98)00190-5.
Honthaas, C., Maury, R. C., Priadi, B., Bellon, H., & Cotten, J. (1999). The Plio–Quaternary Ambon arc, Eastern Indonesia. *Tectonophysics*, *301*(3–4), 261–281.
Hoogewerff, J. A., Van Bergen, M. J., Vroon, P. Z., Hertogen, J., Wordel, R., Sneyers, A., et al. (1997). U-series, Sr-Nd-Pb isotope and trace-element systematics across an active island arc-continent collision zone: Implications for element transfer at the slab-wedge interface. *Geochimica et Cosmochimica Acta*, *61*(5), 1057–1072.
Houseman, G. A., & Gubbins, D. (1997). Deformation of subducted oceanic lithosphere. *Geophysical Journal International*, *131*(3), 535–551.
Hughes, B. D., Baxter, K., Clark, R. A., & Snyder, D. B. (1996). Detailed processing of seismic reflection data from the frontal part of the Timor trough accretionary wedge, eastern Indonesia. *Geological Society, London, Special Publications*, *106*(1), 75–83.
Hung, S.-H., Dahlen, F. A., & Nolet, G. (2000). Fréchet kernels for finite-frequency traveltimeséII. Examples. *Geophysical Journal International*, *141*(1), 175–203. https://doi.org/10.1046/j.1365-246X.2000.00072.x
Kárason, H., & Van Der Hilst, R. D. (2000). Constraints on mantle convection from seismic tomography. *Geophysical Monograph*, *121*, 277–288.
Karig, D. E., Barber, A. J., Charlton, T. R., Klemperer, S., & Hussong, D. M. (1987). Nature and distribution of deformation across the Banda Arc–Australian collision zone at Timor. *Geological Society of America Bulletin*, *98*(1), 18–32.
Keep, M. & Haig, D. W. (2010). Deformation and exhumation in Timor: Distinct stages of a young orogeny, *Tectonophys*. 483, 93-111.
Kennett, B. L. N., & Engdahl, E. R. (1991). Traveltimes for global earthquake location and phase identification. *Geophysical Journal International*, *105*(2), 429–465.
Kincaid, C., & Sacks, I. S. (1997). Thermal and dynamical evolution of the upper mantle in subduction zones. *Journal of Geophysical Research: Solid Earth*, *102*(B6), 12295–12315.
Kissling, E., Husen, S., & Haslinger, F. (2001). Model parametrization in seismic tomography: a choice of consequence for the solution quality. *Physics of the Earth and Planetary Interiors*, *123*(2), 89–101. https://doi.org/10.1016/S0031-9201(00)00203-X
Kreemer, C., Holt, W. E., Goes, S., & Govers, R. (2000). Active deformation in eastern Indonesia and the Philippines from GPS and seismicity data. *Journal of Geophysical Research: Solid Earth*, *105*(B1), 663–680. https://doi.org/10.1029/1999JB900356
Leech, M. L., Singh, S., Jain, A. K., Klemperer, S. L., & Manickavasagam, R. M. (2005). The onset of India–Asia continental collision: Early, steep subduction required by the timing of UHP metamorphism in the western Himalaya. *Earth and Planetary Science Letters*, *234*(1), 83–97. https://doi.org/10.1016/j.epsl.2005.02.038
Levander, A., Bezada, M. J., Niu, F., Humphreys, E. D., Palomeras, I., Thurner, S. M., et al. (2014). Subduction-driven recycling of continental margin lithosphere. *Nature*, *515*(7526), 253.
McCaffrey, R. (1996). Slip partitioning at convergent plate boundaries of SE Asia. *Geological Society, London, Special Publications*, *106*(1), 3–18.
Meighan, H. E., Pulliam, J., ten Brink, U., & López-Venegas, A. M. (2013). Seismic evidence for a slab tear at the Puerto Rico Trench. *Journal of Geophysical Research: Solid Earth*, *118*(6), 2915–2923. https://doi.org/10.1002/jgrb.50227
Menant, A., Sternai, P., Jolivet, L., Guillou-Frottier, L., & Gerya, T. (2016). 3D numerical modeling of mantle flow, crustal dynamics and magma genesis associated with slab roll-back and tearing: The eastern Mediterranean case. *Earth and Planetary Science Letters*, *442*, 93–107.

Miller, M. S., Gorbatov, A., & Kennett, B. L. N. (2006). Three-dimensional visualization of a near-vertical slab tear beneath the southern Mariana arc. *Geochemistry, Geophysics, Geosystems*, *7*(6), Q06012. https://doi.org/10.1029/2005GC001110

Miller, M. S., Levander, A., Niu, F., & Li, A. (2009). Upper mantle structure beneath the Caribbean-South American plate boundary from surface wave tomography. *Journal of Geophysical Research: Solid Earth*, *114*(B1). https://doi.org/10.1029/2007JB005507

Miller, M. S., O'Driscoll, L. J., Roosmawati, N., Harris, C. W., Porritt, R. W., Widiyantoro, S., et al. (2016). Banda Arc Experiment—Transitions in the Banda Arc-Australian Continental Collision. *Seismological Research Letters*, *87*(6), 1417–1423. https://doi.org/10.1785/0220160124

Minear, J. W., & Toksöz, M. N. (1970). Thermal regime of a downgoing slab and new global tectonics. *Journal of Geophysical Research*, *75*(8), 1397–1419.

Mitronovas, W., & Isacks, B. L. (1971). Seismic velocity anomalies in the upper mantle beneath the Tonga-Kermadec island arc. *Journal of Geophysical Research*, *76*(29), 7154–7180.

Nolet, Guust. (1985). Solving or resolving inadequate and noisy tomographic systems. *Journal of Computational Physics*, *61*(3), 463–482.

Nolet, Guust. (1987). Seismic wave propagation and seismic tomography. In *Seismic tomography* (pp. 1–23). Springer. Retrieved from http://link.springer.com/content/pdf/10.1007/978-94-009-3899-1_1.pdf

Nugroho, H., Harris, R., Lestariya, A. W., & Maruf, B. (2009). Plate boundary reorganization in the active Banda Arc–continent collision: Insights from new GPS measurements. *Tectonophysics*, *479*(1), 52–65. https://doi.org/10.1016/j.tecto.2009.01.026

Paige, C. C., & Saunders, M. A. (1982). LSQR: An algorithm for sparse linear equations and sparse least squares. *ACM Transactions on Mathematical Software*, *8*(1), 43–71.

Phillips, W. S., & Fehler, M. C. (1991). Traveltime tomography: A comparison of popular methods. *Geophysics*, *56*(10), 1639–1649.

Poreda, R., & Craig, H. (1989). Helium isotope ratios in circum Pacific volcanic arcs. *Nature*, *338*, 473-478.

Ribe, N. M. (2001). Bending and stretching of thin viscous sheets. *Journal of Fluid Mechanics*, *433*, 135–160.

Richardson, A. N., & Blundell, D. J. (1996). Continental collision in the Banda arc. *Geological Society, London, Special Publications*, *106*(1), 47–60.

Rosenbaum, G., Gasparon, M., Lucente, F. P., Peccerillo, A., & Miller, M. S. (2008). Kinematics of slab tear faults during subduction segmentation and implications for Italian magmatism. *Tectonics*, *27*(2), TC2008. https://doi.org/10.1029/2007TC002143

Royden, L. H., & Husson, L. (2009). Subduction with variations in slab buoyancy: models and application to the Banda and Apennine systems. In *Subduction Zone Geodynamics* (pp. 35–45). Springer.

Sandiford, M. (2008). Seismic moment release during slab rupture beneath the Banda Sea. *Geophysical Journal International*, *174*(2), 659–671. https://doi.org/10.1111/j.1365-246X.2008.03838.x

Saqab, M. M., Bourget, J., Trotter, J. & Keep, M. (2017). New constraints on the timing of flexural deformation along the northern Australian margin: Implications for arc-continent collision and the development of the Timor Trough, *Tectonophys.* 696-697, 14-36.

Sethian, J. A., & Popovici, A. M. (1999). 3-D traveltime computation using the fast marching method. *Geophysics*, *64*(2), 516–523.

Schmandt, B., & Humphreys, E. (2010a). Complex subduction and small-scale convection revealed by body-wave tomography of the western United States upper mantle. *Earth*

and Planetary Science Letters, *297*(3–4), 435–445. https://doi.org/10.1016/j.epsl.2010.06.047

Schmandt, B., & Humphreys, E. (2010b). Seismic heterogeneity and small-scale convection in the southern California upper mantle. *Geochemistry, Geophysics, Geosystems*, *11*(5).

Schöffel, H.-J., & Das, S. (1999). Fine details of the Wadati-Benioff zone under Indonesia and its geodynamic implications. *Journal of Geophysical Research: Solid Earth*, *104*(B6), 13101–13114.

Scire, A., Zandt, G., Beck, S., Long, M., Wagner, L., Minaya, E., & Tavera, H. (2016). Imaging the transition from flat to normal subduction: variations in the structure of the Nazca slab and upper mantle under southern Peru and northwestern Bolivia. *Geophysical Journal International*, *204*(1), 457–479.

Scotney, P.M., Roberts, S., Herrington, R.J., Boyce, A.J. & Burgess, R. (2005). The development of volcanic hosted massive sulfide and barite gold orebodies on Wetar Island, Indonesia. *Mineralium Deposita*, 40 (1), 76-99.

Shulgin, A., Kopp, H., Mueller, C., Lueschen, E., Planert, L., Engels, M., Flueh, E. R., Krabbenhoeft, A. & Djajadihardja, Y. (2009). Sunda-Banda arc transition: Incipient continent-island arc collision (northwest Australia), *Geophys. Res. Lett.* 36. doi:10.1029/2009GL037533.

Silver, E. A., Case, J. E., & Macgillavry, H. J. (1975). Geophysical Study of the Venezuelan Borderland. *Geological Society of America Bulletin*, *86*(2), 213–226. https://doi.org/10.1130/0016-7606(1975)86<213:GSOTVB>2.0.CO;2

Spakman, W., & Nolet, G. (1988). Imaging algorithms, accuracy and resolution in delay time tomography. In *Mathematical geophysics* (pp. 155–187). Springer.

Spakman, Wim. (1991). Delay-time tomography of the upper mantle below Europe, the Mediterranean, and Asia Minor. *Geophysical Journal International*, *107*(2), 309–332. https://doi.org/10.1111/j.1365-246X.1991.tb00828.x

Spakman, Wim, & Hall, R. (2010). Surface deformation and slab–mantle interaction during Banda arc subduction rollback. *Nature Geoscience*, *3*(8), 562–566. https://doi.org/10.1038/ngeo917

Spakman, Wim, & Wortel, R. (2004). A tomographic view on western Mediterranean geodynamics. In *The TRANSMED atlas. The Mediterranean region from crust to mantle* (pp. 31–52). Springer.

Spakman, Wim, van der Lee, S., & van der Hilst, R. (1993). Travel-time tomography of the European-Mediterranean mantle down to 1400 km. *Physics of the Earth and Planetary Interiors*, *79*(1–2), 3–74.

Tate, G. W., McQuarrie, N., van Hinsbergen, D. J. J., Bakker, R. R., Harris, R., Willett, S., et al. (2014). Resolving spatial heterogeneities in exhumation and surface uplift in Timor-Leste: Constraints on deformation processes in young orogens. *Tectonics*, *33*(6), 2013TC003436. https://doi.org/10.1002/2013TC003436

Tate, G. W., McQuarrie, N., van Hinsbergen, D. J., Bakker, R. R., Harris, R., & Jiang, H. (2015). Australia going down under: Quantifying continental subduction during arc-continent accretion in Timor-Leste. *Geosphere*, *11*(6), 1860–1883.

ten Brink, U. S., Shimizu, N., & Molzer, P. C. (1999). Plate deformation at depth under northern California: Slab gap or stretched slab? *Tectonics*, *18*(6), 1084–1098.

Tikhonov, A. N. (1963). On the solution of ill-posed problems and the method of regularization. In *Doklady Akademii Nauk* (Vol. 151, pp. 501–504). Russian Academy of Sciences.

Trampert, J. (1998). Global seismic tomography: the inverse problem and beyond. *Inverse Problems*, *14*(3), 371.

Tregoning, P., Brunner, F. K., Bock, Y., Puntodewo, S. S. O., McCaffrey, R., Genrich, J. F., et al. (1994). First geodetic measurement of convergence across the Java Trench. *Geophysical Research Letters*, *21*(19), 2135–2138. https://doi.org/10.1029/94GL01856

van Hunen, J., & Allen, M. B. (2011). Continental collision and slab break-off: A comparison of 3-D numerical models with observations. *Earth and Planetary Science Letters*, *302*(1), 27–37. https://doi.org/10.1016/j.epsl.2010.11.035

van Keken, P. E., Kiefer, B., & Peacock, S. M. (2002). High-resolution models of subduction zones: Implications for mineral dehydration reactions and the transport of water into the deep mantle. *Geochemistry, Geophysics, Geosystems*, *3*(10), 1–of.

VanDecar, J. C., & Crosson, R. S. (1990). Determination of teleseismic relative phase arrival times using multi-channel cross-correlation and least squares. *Bulletin of the Seismological Society of America*, *80*(1), 150–169.

Vroon, P.Z., Lowry, D., van Bergen, M.J., Boyce, A.J. & Mattey, D.P. 2001. Oxygen isotope systematics of the Banda Arc: low 18O despite involvement of subducted continental material in magma genesis. *Geochemica et Cosmochimica Acta*, 65 (4), 589-609.

Vroon, P. Z., van Bergen, M. J., White, W. M., & Varekamp, J. C. (1993). Sr-Nd-Pb isotope systematics of the Banda Arc, Indonesia: Combined subduction and assimilation of continental material. *Journal of Geophysical Research: Solid Earth*, *98*(B12), 22349–22366. https://doi.org/10.1029/93JB01716

Widiyantoro, S., Pesicek, J. D., & Thurber, C. H. (2011). Subducting slab structure below the eastern Sunda arc inferred from non-linear seismic tomographic imaging. *Geological Society, London, Special Publications*, *355*(1), 139–155.

Widiyantoro, Sri, & van der Hilst, R. (1996). Structure and evolution of lithospheric slab beneath the Sunda arc, Indonesia. *Science*, *271*(5255), 1566–1570.

Widiyantoro, Sri, & van der Hilst, R. (1997). Mantle structure beneath Indonesia inferred from high-resolution tomographic imaging. *Geophysical Journal International*, *130*(1), 167–182.

Wortel, M. J. R., & Spakman, W. (2000). Subduction and Slab Detachment in the Mediterranean-Carpathian Region. *Science*, *290*(5498), 1910–1917. https://doi.org/10.1126/science.290.5498.1910

Zenonos, A., De Siena, L., Widiyantoro, S., & Rawlinson, N. (2019). P and S wave travel time tomography of the SE Asia-Australia collision zone. *Physics of the Earth and Planetary Interiors*, *293*, 106267.

Zhao, L., Jordan, T. H., & Chapman, C. H. (2000). Three-dimensional Fréchet differential kernels for seismic delay times. *Geophysical Journal International*, *141*(3), 558–576. https://doi.org/10.1046/j.1365-246x.2000.00085.x

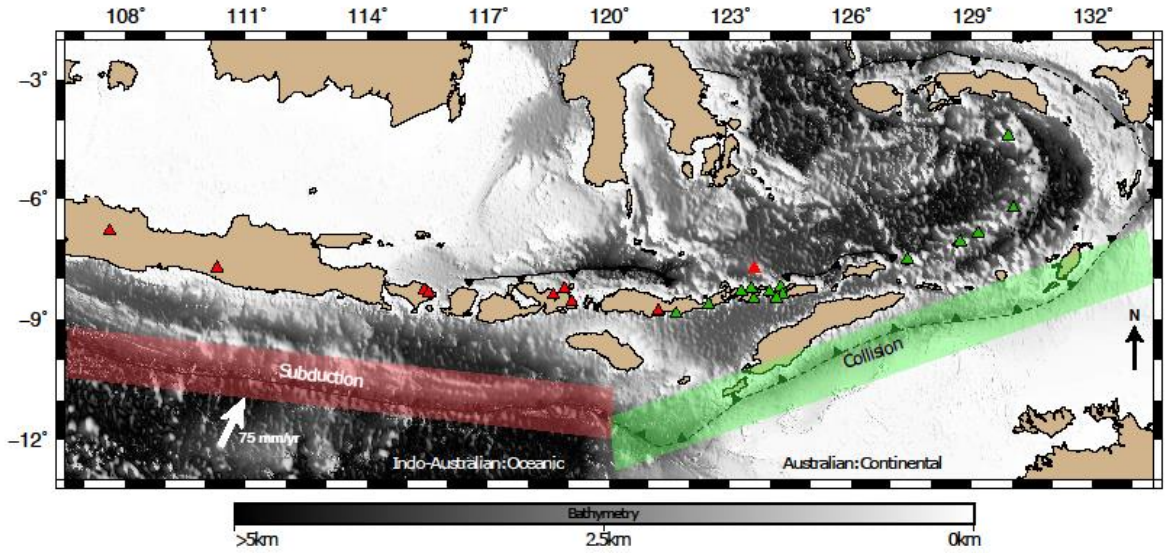

Figure 1. Region of interest. Topography and bathymetry are plotted per the color scale below, courtesy of NASA (e.g. Farr et al., 2007). Volcanoes are colored by He^3/He^4 ratios compared to the same ratio measured in air (R_A). All measurements come from Hilton and Craig (1989), Poreda and Craig (1989), Hilton *et al*. (1992), and Gasparon *et al*. (1994). Volcanoes with ratios below 4 R_A (indicating continental contamination) are plotted in green whereas volcanoes with higher ratios are plotted in red. Inter-plate convergence is indicated with an arrow (Nugroho et al., 2009). The subduction-collision boundary corresponds to the ocean-continent boundary in the subducting lower plate. For this figure and others, plate boundaries are plotted as thin black lines from Bird (2003) and the continental convergent boundary (i.e. collision zone) is plotted as a dashed line.

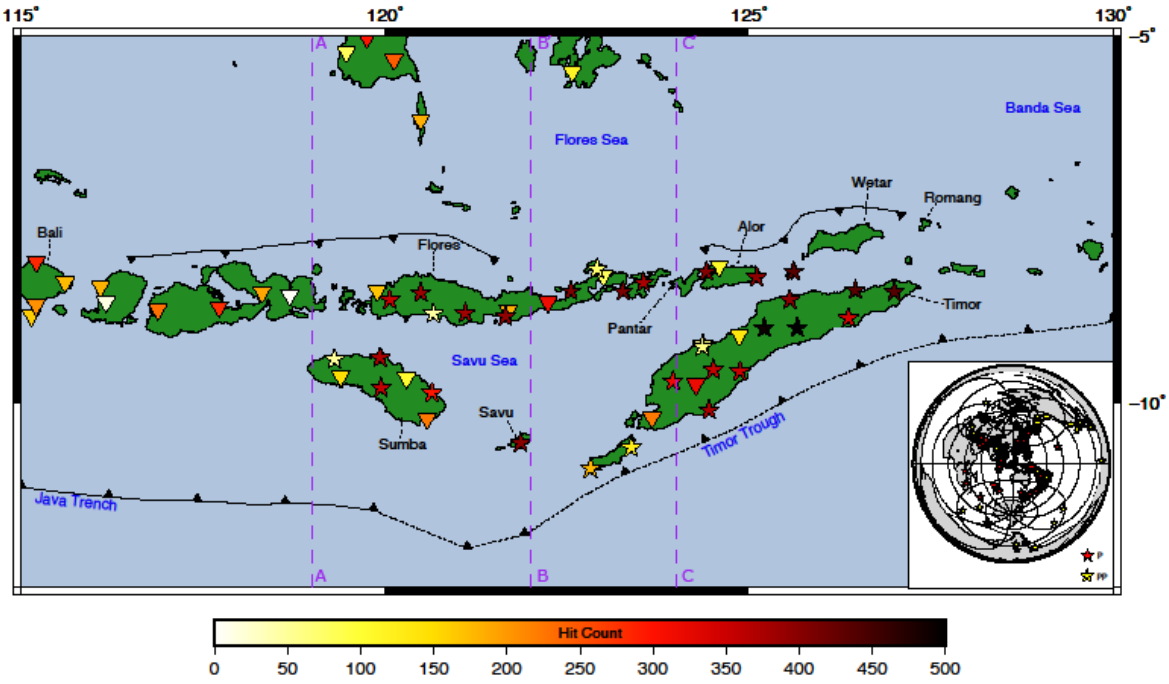

Figure 2. Seismic array. Stations provided by BMKG are plotted as inverted triangles. Stations in temporary USC deployment are plotted as stars. All stations are colored by number of data points (hit count). Geographic features are labeled for reference. Transects are drawn to indicate the longitudinal slices displayed in Figure 6. *Inset*: Earthquakes used in this study. Epicenters are plotted as stars on a polar projection.

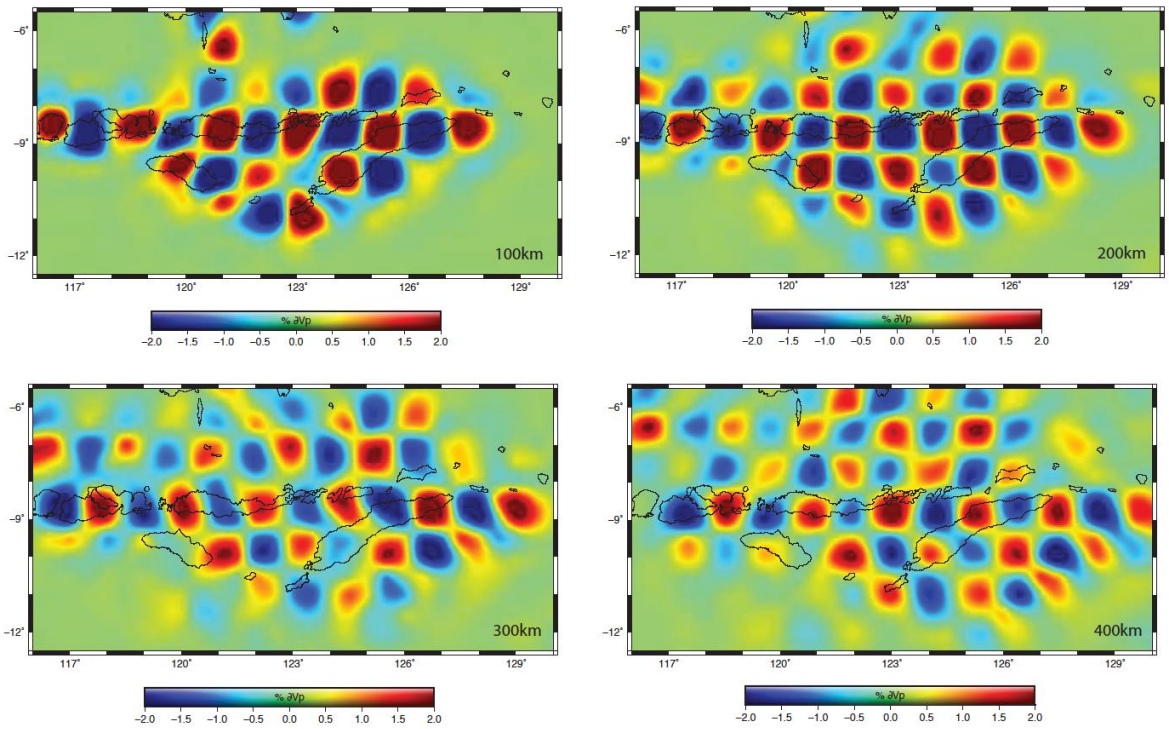

Figure 3. Checkerboard test to assess model resolution. Input pattern consists of 1º x 1º x 150km prisms of alternating ±5% ∂Vp as described in text. Slices are plotted at the depth indicated in the panel. All panels have the same color scale.

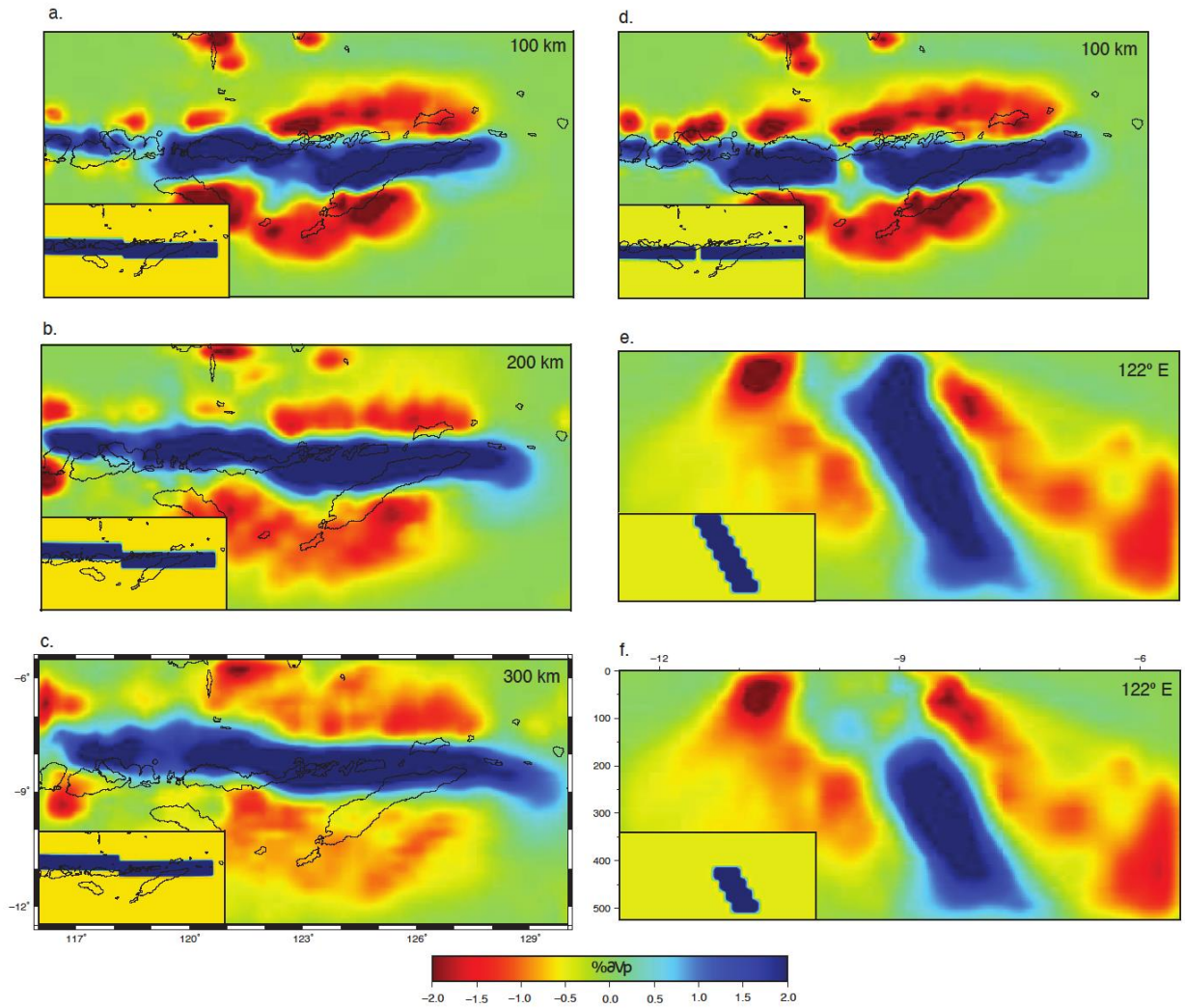

Figure 4. Synthetic resolution tests. Input models are inset in each panel, recovered tomograms are plotted per the color scale at the bottom. In all panels, the input slab was uniformly +5% ∂Vp and the model was demeaned prior to the synthetic inversion procedure. **A-C**: The input model consists of a steeply dipping slab in the east and a western slab with a shallower dip above 200 km and a steep dip > 200 km, similar to what we observe in our actual model. **D-E**: The input consists of a uniformly dipping slab that spans the arc and has a 50 km wide gap above 200 km at the ocean-continent boundary. **F**: The same uniformly dipping slab but with no gap.

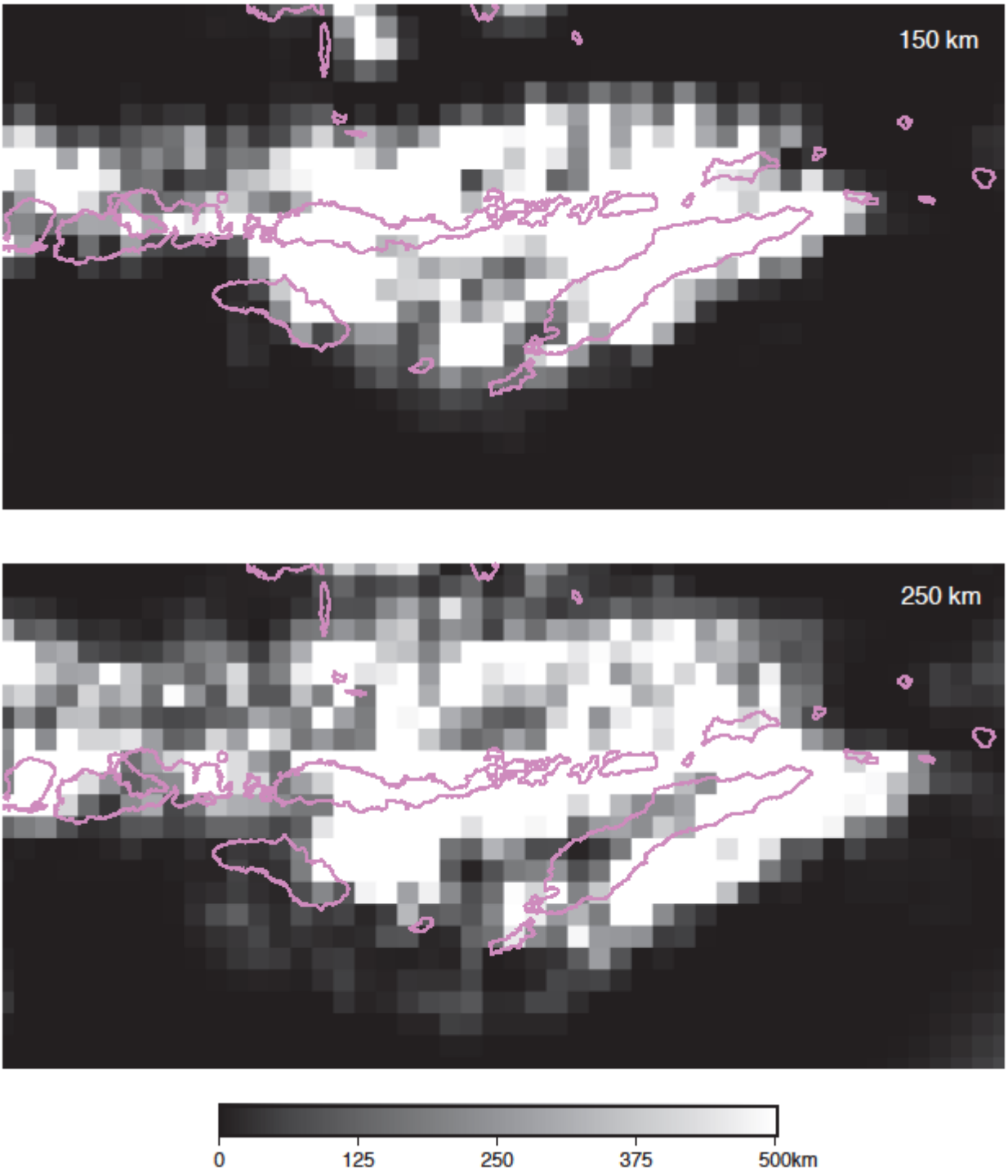

Figure 5. Visualization of ray sampling at 150 km and 250 km depth. Voxels are colored by total ray length over all data points per the color scale (in km) below the panel.

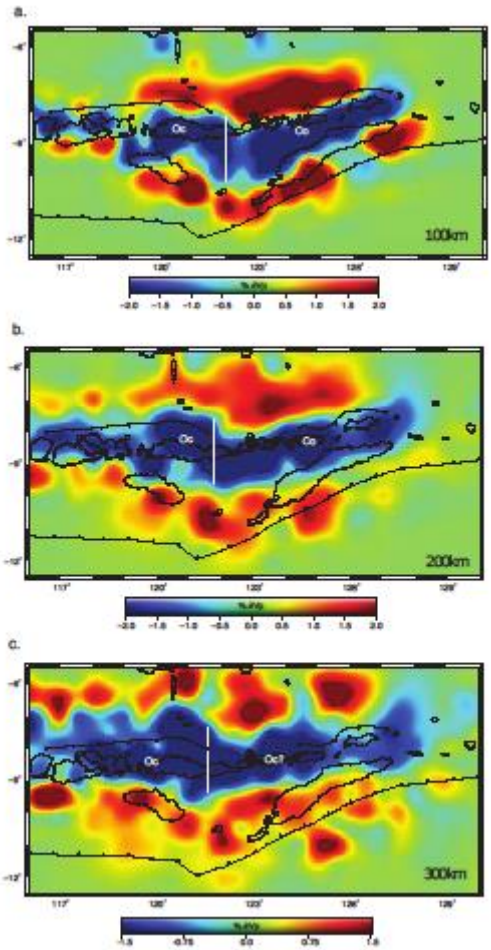

Figure 6. Depth slices of the tomographic model plotted at the depth indicated in the lower right of each panel. All slices display relative P-wave velocity perturbation (%∂Vp) and are plotted using the variable color scale beneath each panel. All slices are demeaned so the total perturbation value is 0 for any given depth. A dashed line is drawn on slices taken at 100, 200, and 300 km depth to indicate the offset between the oceanic (Oc) and continental (Co) sections of the slabs, which are labeled within the panels.

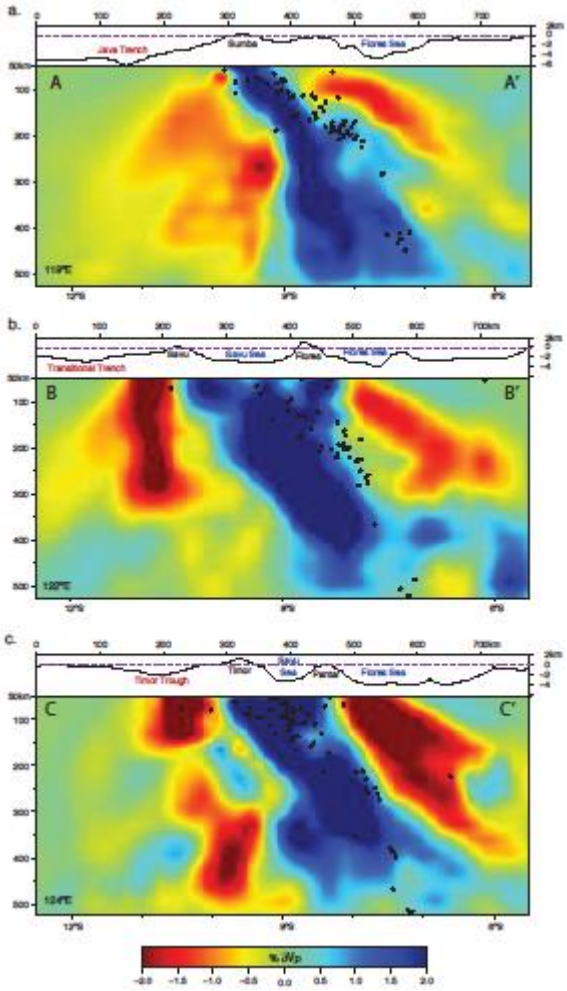

Figure 7. Longitudinal cross-sections through the velocity model. All slices display relative P-wave velocity perturbation (%∂Vp) and are plotted using the same color scale at the bottom. Earthquake hypocenters ± 1º (https://earthquake.usgs.gov/earthquakes/search/) in longitude are plotted as white dots on the cross sections to indicate the general agreement between the fast structure in our model and slab seismicity. Topography/bathymetry from NASA is plotted as a profile atop each cross-section (Farr et al., 2005). Cross sections correspond to purple dashed lines in Figure 2.

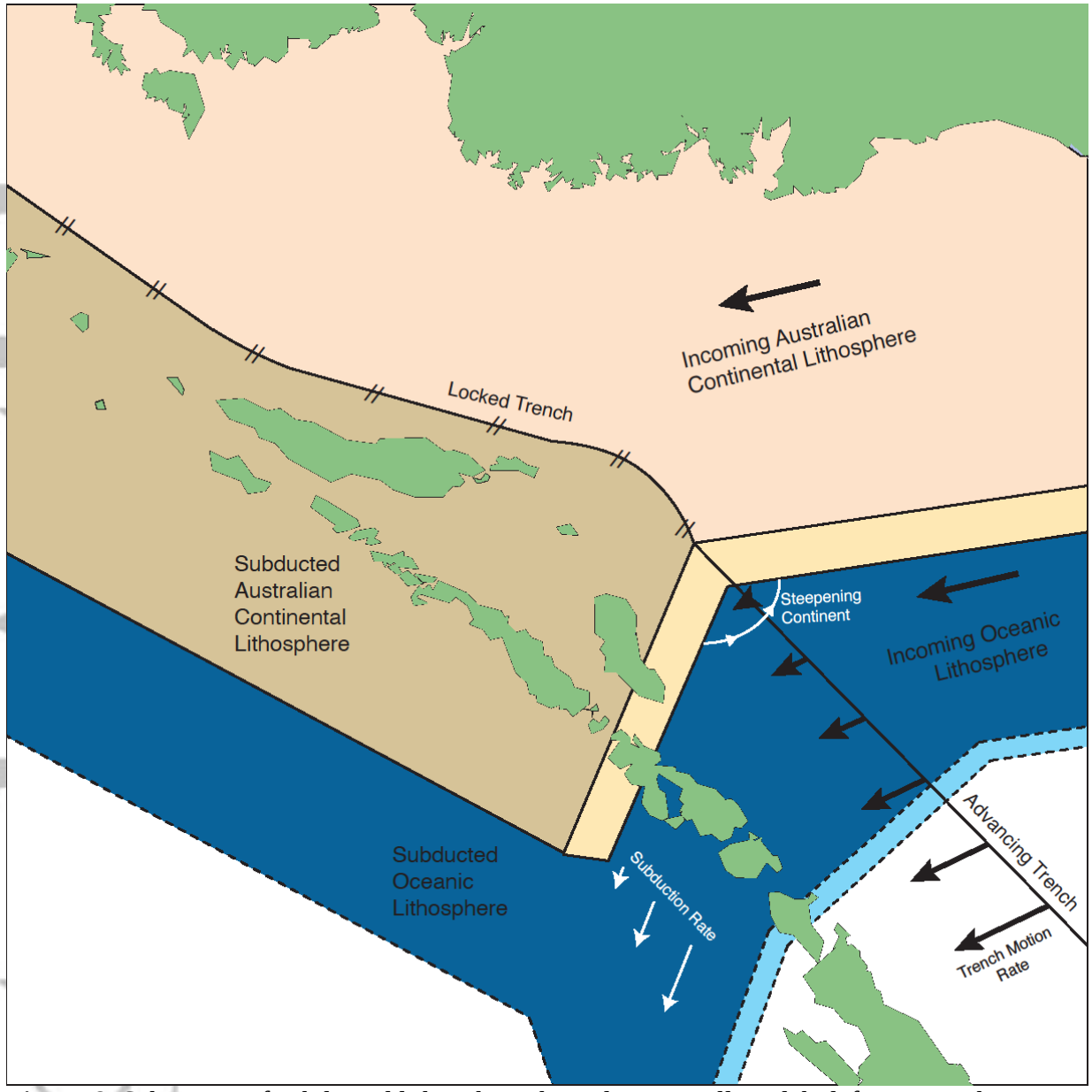

Figure 8. Schematic of subducted lithospheric boundary as well as slab deformation that accommodates the kinematic shift from subduction to collision. The subducted oceanic slab is deforming vertically, to accommodate a gradient in subduction rate, as well as horizontally, to accommodate a difference in trench motion across subduction-collision transition. The locked section of the continental convergent boundary and the advancing trench are indicated with dashes and arrows, respectively, and are based on the plate motion model of Heuret and Lallemand (2005).

Table 1. Table summarizing input data and model dimensions. Data are divided into groups based on network, phase, and frequency band.

	Node Count	Node Spacing	Min Value	Max Value
Longitude	65	~25 km	116º E	130º E

Latitude	33	~25 km	12.5º S	5.5º S
Radius	17	~30 km	5846 km	6371 km
Total	36465			

Table 2. Table summarizing the model space. Model span, number of elements, and spacing are listed.

Network	Phase	Low Pass (Hz)	High Pass (Hz)	Bandpass ID	Datapoints
YS	P	0.02	0.1	b1	3170
YS	P	0.1	0.4	b2	2767
YS	P	0.4	0.8	b3	2461
YS	P	0.8	2.0	b4	1006
BMKG	P	0.7	2.0	b5	10117
YS	PP	0.02	0.1	b1	307
YS	PP	0.1	0.4	b2	127
				Total	19955